Influence of inelastic buckling on low-cycle fatigue degradation of reinforcing bars

Mohammad M. Kashani[1], Aneeka K. Barmi[2], Viktoria S. Malinova[3]

Abstract

The effect of inelastic buckling on low-cycle high amplitude fatigue life of reinforcing bars is investigated experimentally. Ninety low-cycle fatigue tests on reinforcing bars varied in amplitudes and buckling lengths are conducted. Using scanning electron microscope the fractography of fractured surfaces are studied. The results show that the inelastic buckling, bar diameter and surface condition are the main parameters affecting the low-cycle fatigue life of reinforcing bars. Through nonlinear regression analyses of the experimental data a new set of empirical equations for fatigue life prediction of reinforcing bars as a function of the buckling length and yield strength are developed. Finally, these empirical models have been implemented into a new phenomenological hysteretic material model for reinforcing bars. The new material model is able to simulate the nonlinear stress-strain behaviour of reinforcing bars with the effect of inelastic buckling and low-cycle fatigue degradation. The results of simulation using the analytical model show a good agreement with the observed experimental results.

Keywords: Low-cycle fatigue, buckling, cyclic behaviour, reinforcing steel, stress-strain relation

[1]Lecturer, University of Bristol, Dept. of Civil Engineering University of Bristol, Bristol, BS8 1TR, United Kingdom (corresponding author), E-mail: mehdi.kashani@bristol.ac.uk
[2]MEng Student, University of Bristol, Dept. of Civil Engineering University of Bristol, Bristol, BS8 1TR, United Kingdom
[3]MEng Student, University of Bristol, Dept. of Civil Engineering University of Bristol, Bristol, BS8 1TR, United Kingdom

1. Introduction

The current performance-based seismic design philosophy of reinforced concrete (RC) structures relies on the proper detailing of plastic hinge regions where most of the inelastic deformations are expected to occur. The inelastic cyclic deformation in plastic hinge regions results in a significant tension and compression strain reversals. Among RC concrete components, RC bridges piers are the most vulnerable components. This is because the structural system of bridges is very simple (a single degree of freedom system). Unlike buildings where plastic hinges are designed to occur in beams, due to the nature of the structural system of bridges the plastic hinges are forced to occur in piers. As a result, they should be able to accommodate a significant inelastic deformation due to earthquake loading. Therefore, several researchers have studied the nonlinear behaviour of RC components under cyclic loading [1,2]. In these studies fracture of vertical reinforcing bars in RC columns under cyclic loading has been observed [1,2] which is due to the low-cycle high amplitude fatigue degradation of vertical reinforcing bars.

Moreover, there is a large number of existing bridges around the world that were designed prior to the modern seismic design codes and therefore they are not properly detailed for seismic loading. One of the most common type of failure mode of RC bridge piers that has been observed in real earthquakes and experimental testing is the buckling of vertical reinforcement which is then followed by fracture of reinforcement in tension due to low-cycle high amplitude fatigue degradation [1,2,3]. Therefore, several researchers have investigated the nonlinear cyclic behaviour of reinforcing bars with the effect of inelastic buckling [4-12]. The experimental results showed that the inelastic buckling has a great influence on low-cycle fatigue life of reinforcing bars. More recently Kashani [13] investigated the nonlinear behaviour of RC bridge piers numerically and compared with the experimental data reported in [1,2]. They have reported that the buckling length of

longitudinal reinforcing bars in RC columns has a significant impact of the fracture of these bars in tension. However, despite the previous research in this area, there has not been any experimental study to explore and quantify the significance of inelastic buckling on low-cycle fatigue life of reinforcing bars.

This paper is addressing this issue and explores the impact of inelastic buckling on low-cycle fatigue life of reinforcing bars. Therefore, a comprehensive experimental testing conducted on ninety reinforcing bars under low-cycle fatigue strain history varied in buckling lengths (slenderness ratio), diameters, yield strengths and surface roughness (ribbed and smooth bars). Using the scanning electron microscope (SEM) a fractography analysis of the fractured surfaces are conducted. Finally, using the experimental results a set of empirical models are developed to predict the low-cycle fatigue life of reinforcing bars as a function of buckling length and yield strength.

Moreover, earlier research by Kashani [13] resulted in development of a new phenomenological hysteretic material model for reinforcing bars which is implemented in the OpenSees [14] an open source finite element code for nonlinear seismic analysis of structures. This model is capable of simulating the nonlinear cyclic behaviour of reinforcing bars with the effect of inelastic buckling and low-cycle fatigue degradation. However, due to the paucity of experimental data in the literature, the fatigue material parameters have not been calibrated to account for the influence of buckling on low-cycle fatigue degradation of reinforcing bars. The experimental data and empirical models in this paper helped to improve this feature of Kashani's model. The results of the improved analytical model are in a good agreement with the observed experimental results. Moreover, this model is readily available in the OpenSees to be used by the earthquake engineering community for nonlinear seismic analysis of RC bridges/structures.

2. Experimental programme

A total of ninety test specimens are prepared for low-cycle high amplitude fatigue tests. The reinforcement used in this experiment are B500B ribbed and B460 smooth British manufactured reinforcing bars [15]. The specimens are including thirty 12mm diameter ribbed reinforcing bars, thirty 16mm diameter ribbed reinforcing bars and thirty 12mm diameter smooth reinforcing bars. For each group of test specimens three tension tests are conducted to evaluate the material properties. Table 1 summarises the material properties of test specimens and Fig. 1 shows the typical stress-strain curve for each group of test specimens.

Table 1 Mechanical properties of tests specimens

		16mm Ribbed	12mm Ribbed	12mm Smooth
Yield strain	ε_y	0.0027	0.0028	0.0023
Yield stress (MPa)	σ_y	535.67	544.33	474.5
Elastic modulus (MPa)	E_s	200000	191666.67	204500
Hardening strain	ε_{sh}	0.0183	0.0287	0.0046
Strain at maximum stress	ε_u	0.104	0.143	0.061
Maximum stress (MPa)	σ_u	633.75	640.67	510.564
Fracture strain	ε_r	0.195	0.222	0.54185

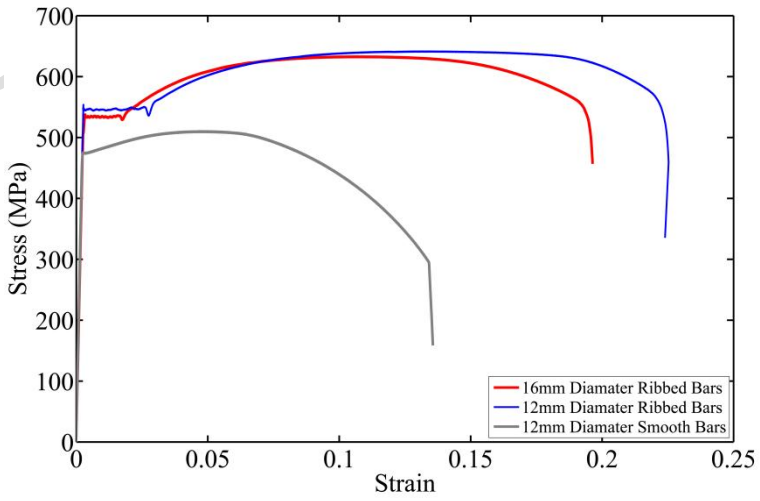

Fig. 1. Stress-strain behaviour of test specimens in tension

2.1. Low-cycle high amplitude fatigue test

A total of ninety low-cycle fatigue tests are conducted on reinforcing bars with different buckling lengths and strain amplitudes. It is well known that the buckling length of the vertical reinforcing bars inside RC columns is a function of the stiffness of horizontal tie reinforcement [13]. Therefore, slenderness ratios for the experiment are chosen based on the common observed buckling modes of vertical reinforcement in RC columns as report in [13]. The slenderness ratio is defined by the L/D ratio where L is the length and D is the bar diameter. The L/D ratios tested in this experiment are 5, 8, 10, 12 and 15.

A 250kN universal testing machine with hydraulic grips was used for the low-cycle fatigue testing of the reinforcing bars. The machine used an integral Linear Variable Displacement Transducer (LVDT) to measure the displacement of the grips. A displacement control loading protocol with zero mean strain using a sine wave loading pattern with constant amplitude is used in the low-cycle fatigue tests. The strain rate is set to 0.005strain/sec throughout the experiment. The total strain amplitudes used in the low-cycle fatigue tests are 1%, 1.5% 2%, 3%, 4% and 5% for 12mm diameter bars and 1%, 1.5% 2%, 2.5% 3% and 4% for 16mm diameter bars. A picture of the three groups of bars used in the low-cycle fatigue tests is shown in Fig. 2. It should be noted that the failure of the specimen is taken to be the point at which the bar is completely fractured.

Fig. 2. Low-cycle fatigue test specimens

3. Experimental results and discussion

3.1. Influence of inelastic buckling and slenderness ratio

Fig. 3 shows an example hysteretic response of 12mm ribbed bars under low-cycle fatigue test at 5% strain amplitude. Fig. 3 (a) shows that hysteretic response of the bars with L/D = 5 are almost symmetrical in tension and compression. However, as the slenderness ratio of bars increases a pinching response is observed which is due to the impact of inelastic buckling and geometrical nonlinearity on the hysteretic response. The results show that the fatigue induced crack initiation in the group of bars with L/D = 10 and 15 is much quicker than the group of bars with L/D = 5. Moreover, It was observed that crack always started at the inside face of the buckle bar. This is because, when a bar buckles the total strain amplitude at inside face of the bar increases due to the combined axial and bending deformation which is known as second order effect. Therefore, the low-cycle fatigue has a more severe effect in bars with larger L/D ratio. Fig. 4 shows an example of fractured bars after low-cycle fatigue test.

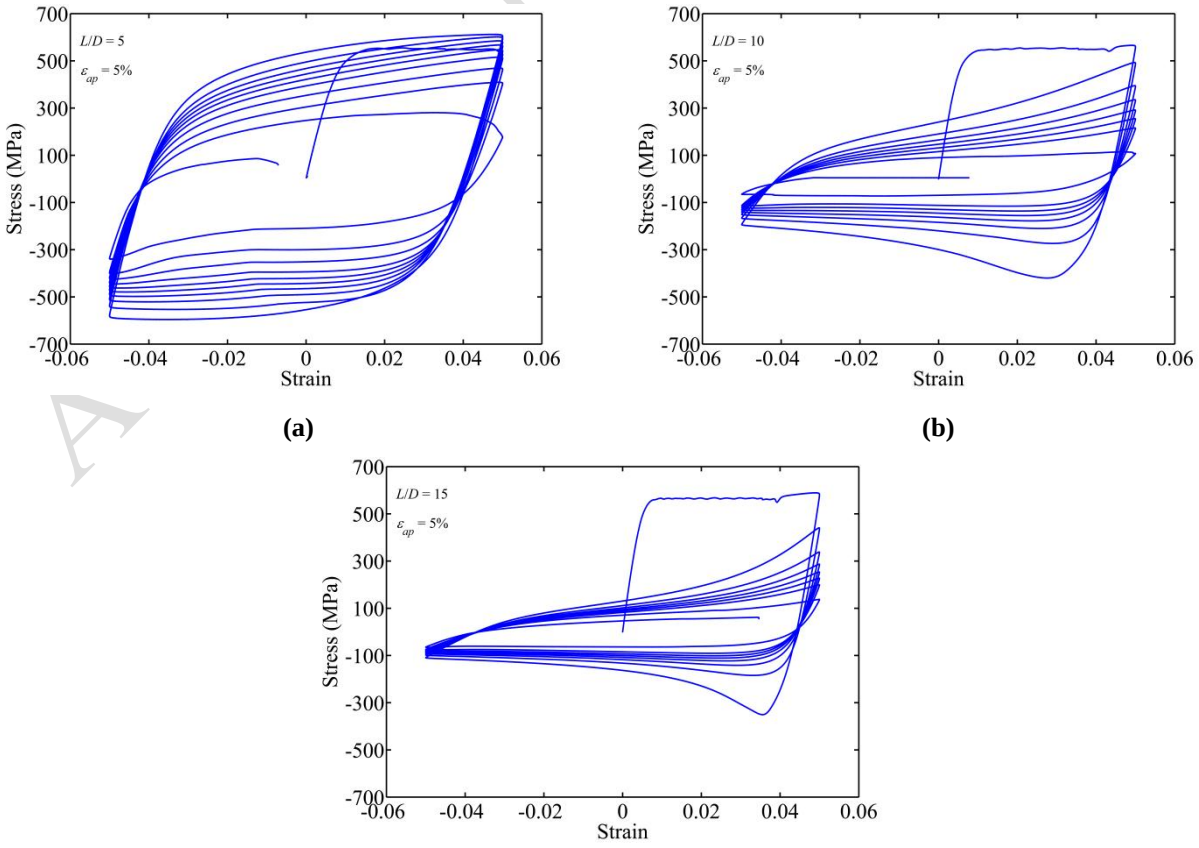

(a)

Fig. 3. Hysteretic response of 12mm ribbed reinforcing bars: (a) L/D = 5, (b) L/D = 10, (c) L/D = 15

Fig. 4. Buckled shape of a 12mm diameter bar with L/D = 15 after failure

In order to show the impact of buckling on low-cycle fatigue degradation of reinforcing bars a comparison is made between the total energy dissipation and cyclic stress degradation of different groups of bars. Fig. 5 shows the normalised total hysteretic energy for ribbed bars with 12mm and 16mm diameter and varied in slenderness ratios and strain amplitudes. The variable E_t is the total hysteretic energy of bars in low-cycle fatigue test and E_y is the elastic energy of the corresponding bars under monotonic tension.

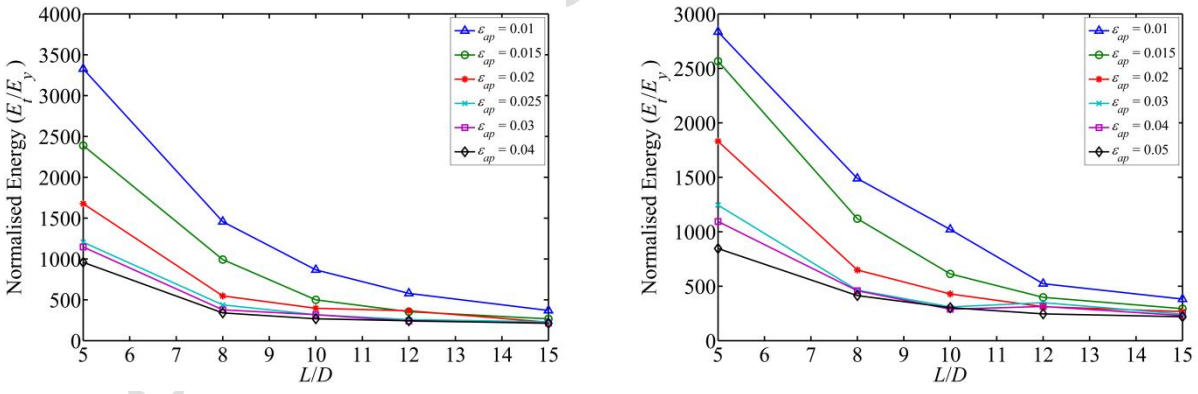

(a) **(b)**

Fig. 5. Normalised dissipated hysteretic energy: (a) 16mm ribbed bars (b) 12mm ribbed bars

As it is shown in Fig. 5, buckling has a more significant impact on energy dissipation at lower strain amplitude. As the strain amplitude increases beyond 2.5% almost all of the bars with $L/D \geq 8$ converge towards the same point.

Fig. 6 shows example graphs of the cyclic stress loss of 16mm diameter bars under low-cycle fatigue test with 4% strain amplitude. It should be noted that the normalised stress in Fig. 6 is the value of the stress at the pick strain amplitude in tension and compression in each half cycle normalised to the yield stress. Fig. 6 (a) shows that the stress loss in tension and compression is almost symmetrical for bars with L/D = 5. Given a zero mean strain history is used in the experiment, as expected, the mean stress loss is almost zero in bars with L/D = 5. However, as it is shown in Fig. 6 (b) the normalised stress loss in tension and compression is not symmetrical for bars with L/D = 15. This results in moving the normalised mean stress graph from zero. This indicates that buckling increases the stress loss of reinforcing bars in compression under cycling loading. Moreover, Fig. 6 (b) shows that the stress loss in tension much faster than bars with L/D =5.

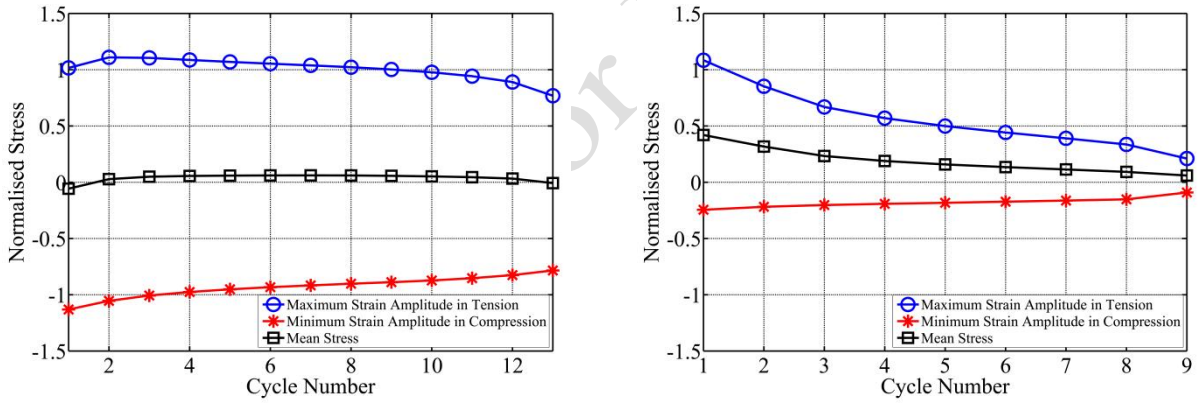

Fig. 6. Stress degradation of 16mm ribbed bars: (a) L/D = 5, 4% strain amplitude (b) L/D = 15, 4% strain amplitude

3.2. Influence of bar diameter

The observed hysteretic responses of 12mm and 16mm diameter bars with L/D = 5 and 15 are shown in Fig. 7. It is clear that the diameter does not have a significant impact of hysteric response and buckling behaviour of reinforcing bars.

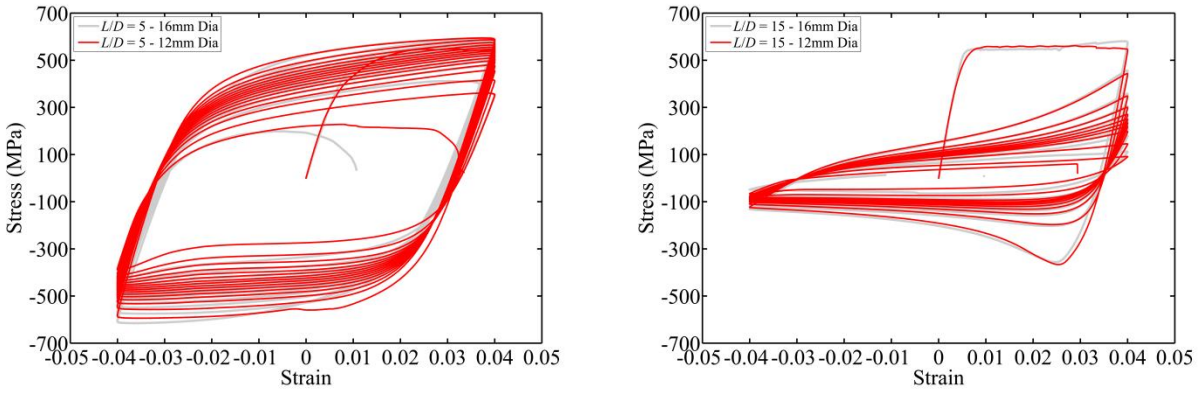

(a) (b)

Fig. 7. Hysteretic response of reinforcing bars with different diameter and slenderness ratio: (a) *L*/*D* = 5, 12mm and 16mm Dia (b) *L*/*D* = 15, 12mm and 16mm Dia

Furthermore, Fig. 8(a) shows that the diameter has a very small impact on the total dissipated hysteretic energy. However, Fig. 8(b) shows that although the stress degradation trend is almost the same in 12mm and 16mm diameter bars, the 16mm diameter bars have a shorter fatigue life compare to 12mm diameter bars. This suggests that the larger diameter bars have shorter low-cycle fatigue life.

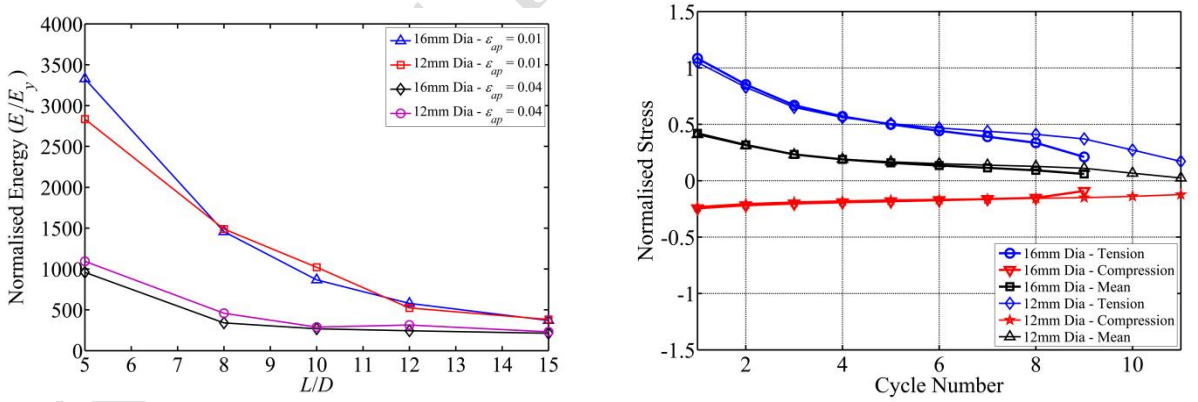

(a) (b)

Fig. 8. Influence of bar diameter on cyclic degradation: (a) Hysteretic energy dissipation and (b) stress degradation (*L*/*D* = 15 at 4% strain amplitude)

3.3. Influence of material type and surface condition

Fig. 9 shows a comparison between the hysteretic responses of 12mm diameter ribbed and smooth bars. Given the yield stress (σ_y) is different in these bars, the stress (σ) is normalised to their corresponding yield stress.

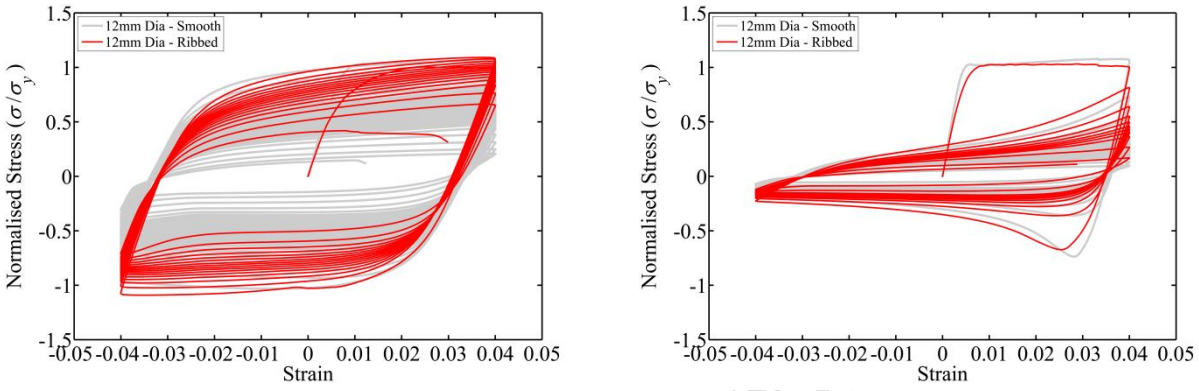

(a) **(b)**

Fig. 9. Hysteretic response of smooth and ribbed bars with 12mm in diameter: (a) *L*/*D* = 5 (b) *L*/*D* = 15

The observed responses in Fig. 9(a) shows that the cyclic stress degradation is much higher in smooth bars compare to ribbed bars in L/D = 5. However, Fig. 9(b) shows that the stress degradation difference between the smooth and ribbed bars is much lower in bars with L/D = 15. Despite the high degradation rate in smooth bars, it is found that the fatigue life of the smooth bars is higher than ribbed bars and their failure mode is more ductile compare to ribbed bars. As slenderness ratio of bars increased the difference in the fatigue life of ribbed and smooth bars became much smaller which is due to the impact of buckling on the low-cycle fatigue life of bars. Fig. 10 shows the total energy loss of 12mm diameter ribbed and smooth reinforcing bars under 4% strain amplitude and varied L/D ratios.

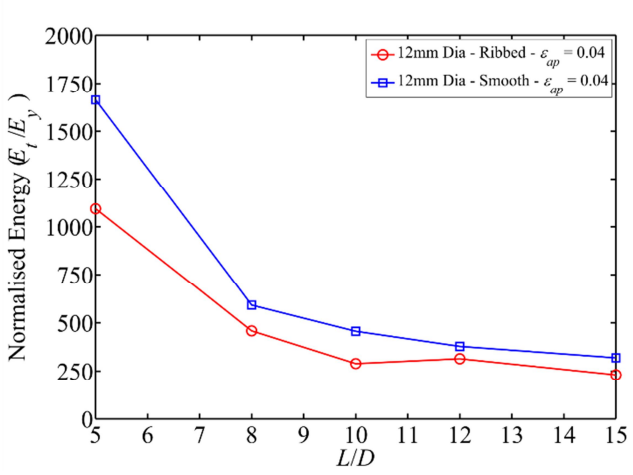

Fig. 10. Comparison of the hysteretic energy dissipation in smooth and ribbed bars

Despite the lower ductility (area under stress-strain curve in tension) of smooth bars in monotonic tension they showed more ductile behaviour under cyclic loading (area inside the cyclic stress-strain curve). This is primarily due to the surface conditions as reported by other researchers [16-19]. [16] reported that the fatigue life of ribbed bars is generally lower than smooth bars due to the stress concentration at the root of the ribs which results in crack initiation at these locations. Therefore, the failure mode is less ductile compare to smooth bars. Fig. 11 shows examples of fractured surfaces of ribbed and smooth bars. Further discussion about the fractured surfaces is available in section 3.4 of this paper.

It can be concluded from Fig. 10 that the surface roughness has a great influence on the fatigue life of reinforcing bars with small *L*/*D* ratio. However, as the *L*/*D* ratio increases the impact of buckling is more severe than the surface roughness and therefore the inelastic buckling has a greater influence on the low-cycle fatigue life of reinforcing bars.

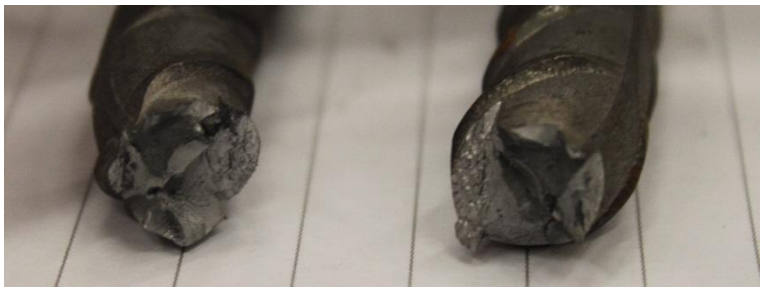

(a)

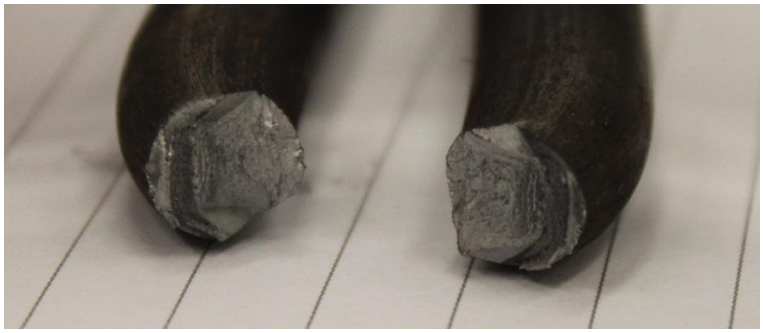

(b)

Fig. 11. Observed fracture surface of 12mm diameter bars after low-cycle fatigue test with 5% strain amplitude: (a) a ribbed bar with L/D = 15 and (b) a smooth bar with L/D = 15

3.4. Fractography of the fractured surfaces using Scanning Electron Microscope (SEM)

SEM was used for fractography of the fractured surfaces. This was used to take detailed images of some sample fractured specimens to investigate the crack propagation by topography of the fractured surface. This apparatus focusses a beam of high energy electrons on to the specimens that interact with the atoms at the surface to produce a detailed scan of the specimen.

As explained in section 3.3, The fatigue crack of the ribbed bars under repeated cyclic loading initiated along the root of the transverse rib on the inside face of the buckled bar. After initiation, the cracks propagated away from the transverse rib on the bar surface into the body of the bar normal to the bar axis. This suggests that the largest stresses lie in the longitudinal direction, as otherwise the cracks would have grown along the along the root where the magnitudes of stress concentrations are much higher than elsewhere. The fatigue crack of the smooth bars also initiated on the inside face of the buckled bar and propagated away from the bar surface into the body of the bar normal to the bar axis. However, the crack initiation and propagation of smooth bars were much slower than ribbed bars. This difference

in the behaviour resulted in more ductile failure of smooth bars compare to ribbed bars with the same L/D ratio and strain amplitude.

Fig. 12 (a-f) shows the fractographs of 12mm ribbed and smooth bars and 16mm ribbed bars with L/D = 15. Comparing Fig. 12(a) and (b) with Fig. 12(c) and (d) shows that the dark areas of striation are associated with slower crack propagation in smooth bars (Fig. 12(c) and (d)) that took longer to fracture and showed more plastic deformation. The lighter areas in ribbed specimens shows a more sudden fracture near the rib root as shown in Fig. 12(a) and (b) and Fig. 12(e) and (f). Moreover, the fracture surface of 16mm diameter ribbed bars in Fig. 12(e) and (f) shows lighter areas than 12mm diameter ribbed bars. This indicates that the diameter of bars increases the facture of bars become less ductile. The discussion of the influence of bar diameter on low-cycle fatigue life of reinforcing bars requires further experimental testing and is an area for future research.

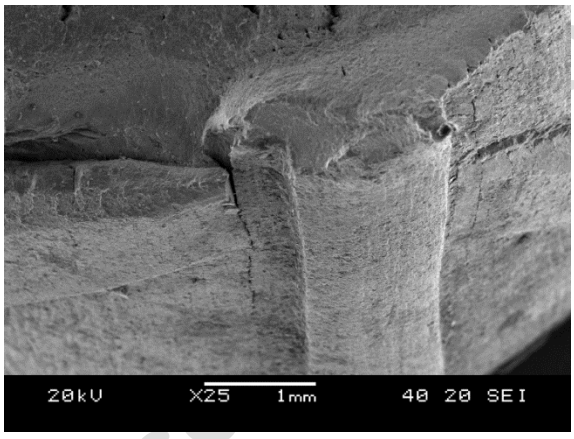

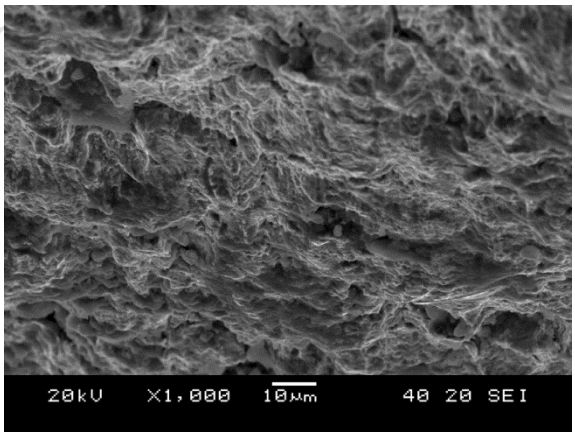

(a) **(b)**

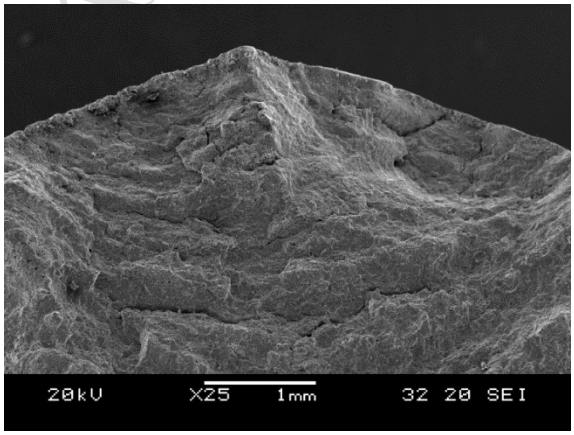

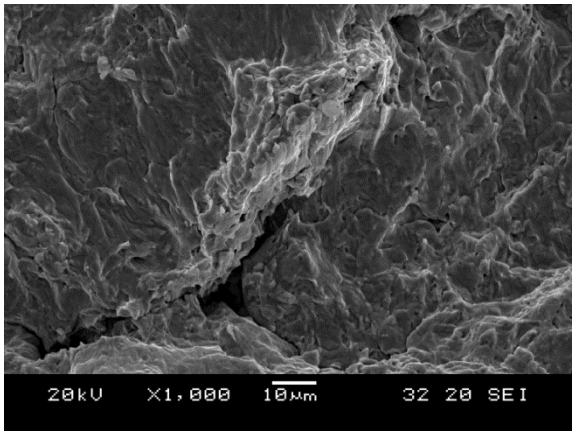

242 **(c)** **(d)**

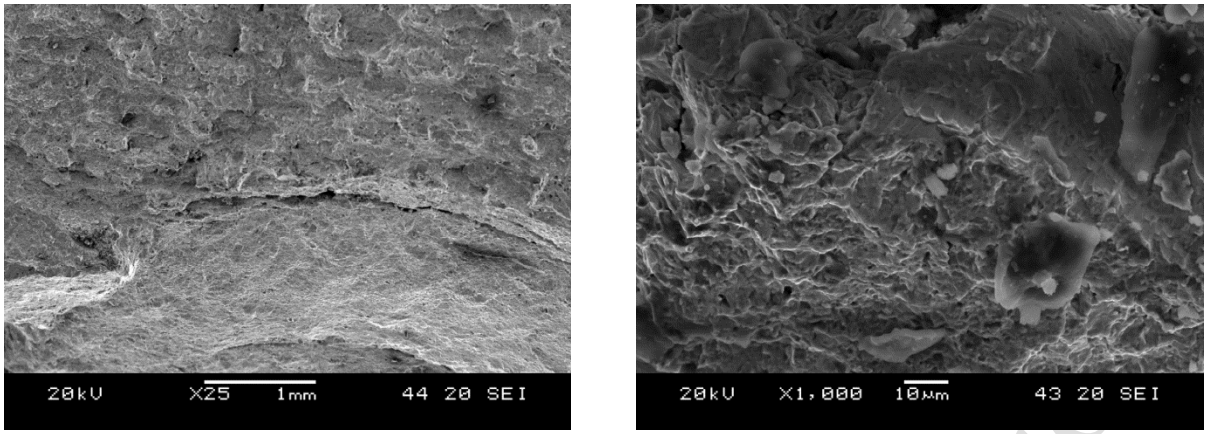

243

244 **(e)** **(f)**

245 **Fig. 12. SEM fractographs of fractured bars with *L*/*D* = 15 after low cycle fatigue tests at 4% strain**
246 **amplitude: (a) and (b) 12mm diameter ribbed bars (c) and (d) 12mm diameter smooth bars (e) and (f)**
247 **16mm diameter ribbed bars**

248 ## 4. Modelling low-cycle fatigue life of reinforcing bars

249 ### 4.1. Basic low-cycle fatigue model using strain life approach

250 The low-cycle fatigue life of reinforcing bars without the effect of buckling has been studied
251 by several researchers [3,16,17,19]. They have mainly used three methods to model the low-
252 cycle fatigue life of reinforcing bars i.e. Coffin-Manson [20], Koh-Stephen [21] and energy
253 method [22]. It should be noted that these models are only valid for low-cycle fatigue under
254 constant amplitude loading. Therefore, Miner's rule [23] can be employed to account for the
255 cumulative damage due to random loading history (further discussion is available in [3,5,7]).

256 Among the aforementioned models, Coffin-Manson and Koh-Stephen are more popular
257 among researchers as they are easy to be implemented to any finite element package for
258 seismic analysis of civil engineering structures such as OpenSees [14].

259 Both Coffin-Manson and Koh-Stephen models are using strain life approach to model the
260 low-cycle fatigue life of engineering materials. The plastic strain amplitude is the most
261 important parameter affecting the low-cycle fatigue life of material. Therefore, Coffin-

Manson model, as described in Eq. (1), relates the plastic strain amplitude (ε_p) to the fatigue life.

$$\varepsilon_p = \varepsilon'_f \left(2N_f\right)^c \tag{1}$$

where, ε'_f is the ductility coefficient i.e. the plastic fracture strain for a single load reversal, c is the ductility exponent and $2N_f$ is the number of half-cycles (load reversals) to failure. Koh-Stephen [21] extended the Coffin-Manson [20] for modelling the low-cycle fatigue life of materials based on the total strain amplitude (elastic strain + plastic strain) as described in Eq. (2).

$$\varepsilon_a = \varepsilon_f \left(2N_f\right)^\alpha \tag{2}$$

where, ε_f is the ductility coefficient i.e. the total fracture strain for a single load reversal, α is the ductility exponent and $2N_f$ is the number of half-cycles (load reversals) to failure.

In this research, the Koh-Stephen model is used to predict the low-cycle fatigue life of reinforcing bars. Furthermore, the influence of inelastic buckling on fatigue material constants ε_f and α is also explored.

Eq. (2) is fitted to the observed experimental data of each slenderness ratio individually to calibrate the fatigue material constants (ε_f and α). The results of the regression analyses are summarised in Table 2. Fig. 13 shows example of the Eq. (2) fitted to the experimental data for three groups of bars using a nonlinear regression analysis.

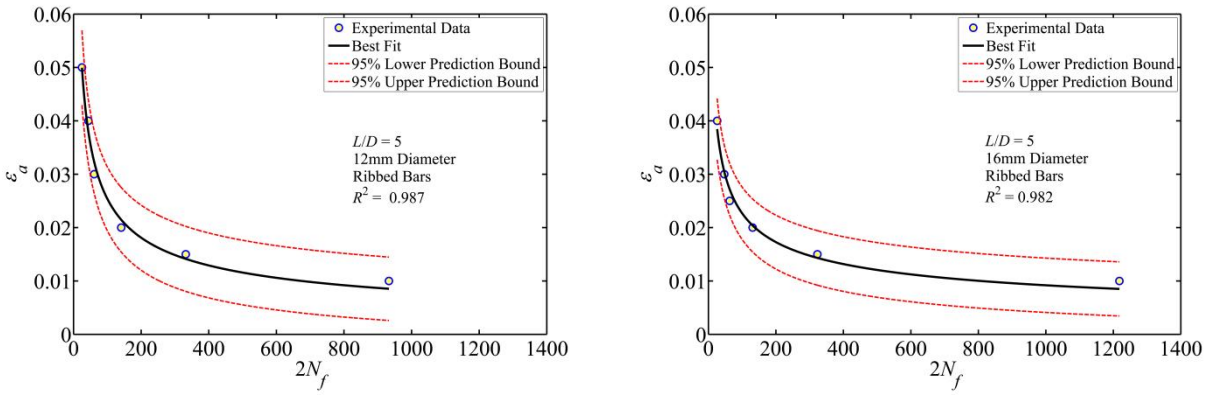

(a) **(b)**

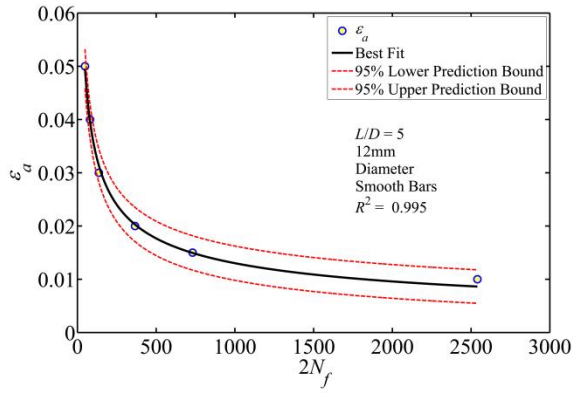

(c)

Fig. 13. Calibration of the fatigue material constant for reinforcing bars with *L*/*D* = 5: (a) 12mm diameter ribbed bars (b) 16mm diameter ribbed bars (c) 12mm diameter smooth bars

Table 2 Results of regression analysis to calibrate the low-cycle fatigue material constants

12mm Ribbed Bars				16mm Ribbed Bars				12mm Smooth Bars			
L*/*D	ε_f	α	R^2	***L*/*D***	ε_f	α	R^2	***L*/*D***	ε_f	α	R^2
5	0.188	-0.448	0.987	5	0.138	-0.393	0.982	5	0.245	-0.491	0.996
8	0.262	-0.608	0.963	8	0.128	-0.470	0.981	8	0.228	-0.565	0.999
10	0.279	-0.660	0.942	10	0.192	-0.602	0.990	10	0.355	-0.715	0.995
12	0.398	-0.734	0.907	12	0.254	-0.677	0.962	12	0.457	-0.772	0.994
15	0.484	-0.799	0.983	15	0.407	-0.810	0.987	15	0.734	-0.907	0.996

4.2. Correlation between the fatigue material constants and inelastic buckling

The inelastic buckling behaviour of reinforcing bars has been investigated by several researchers [4,8,11,6,7,24]. In all of the previous studies researchers have agreed that the post-buckling behaviour of reinforcing bars is affected by yield stress σ_y and geometrical slenderness ratio *L*/*D*. Dhakal-Maekawa [11] found that the post buckling behaviour of reinforcing bars is govern by a single compound variable called non-dimensional bar buckling parameter λ_p as described in Eq. (3).

$$\lambda_p = \sqrt{\frac{\sigma_y}{100}}\frac{L}{D} \tag{3}$$

Where, σ_y is the yield stress and *L*/*D* is the geometrical slenderness ratio of reinforcing bars. It should be noted that the yield stress in Eq. (3) should be in MPa.

Kashani [13] developed a new phenomenological hysteretic model for reinforcing bars that accounts for inelastic buckling and low-cycle fatigue degradation. This model uses the λ_p to define the post-buckling and cyclic response of reinforcing bars. However, the influence of inelastic buckling on the low-cycle fatigue degradation is not currently included in the model. Therefore, in this section the correlation between λ_p and low-cycle fatigue material constants is explored. Further discussion about this model is available in section 5 of this paper.

In this study the Pearson's linear correlation coefficient (ρ) is employed to investigate the correlation of the λ_p and the low-cycle fatigue material constants α and ε_f. The calculated correlation coefficients together with P-values at 0.05 significance are shown in Table 3.

Table 3 Correlation between the fatigue material constants and λ_p

Model Parameter	16mm Ribbed		12mm Ribbed		12mm Smooth	
	α	ε_p	α	ε_p	α	ε_p
Pearson						
ρ	-0.9924	0.9191	-0.9618	0.9887	-0.9569	0.9881
P-value	7.90×10^{-4}	0.0273	0.0089	0.0014	0.0107	0.0016

The results of correlation analysis show that there is a very strong negative correlation between α and λ_p and there is a very strong positive correlation between ε_f and λ_p. This is also clear from the corresponding P-values of the fatigue material constants α and ε_f which are all less than the considered significance level (0.05). This shows that the dependence of the fatigue material constants and λ_p is statistically significant. The interrelationship between the fatigue material constants and the λ_p is modelled using regression analysis of the data. The results of the regression analysis are shown in Fig. 14 (a-f).

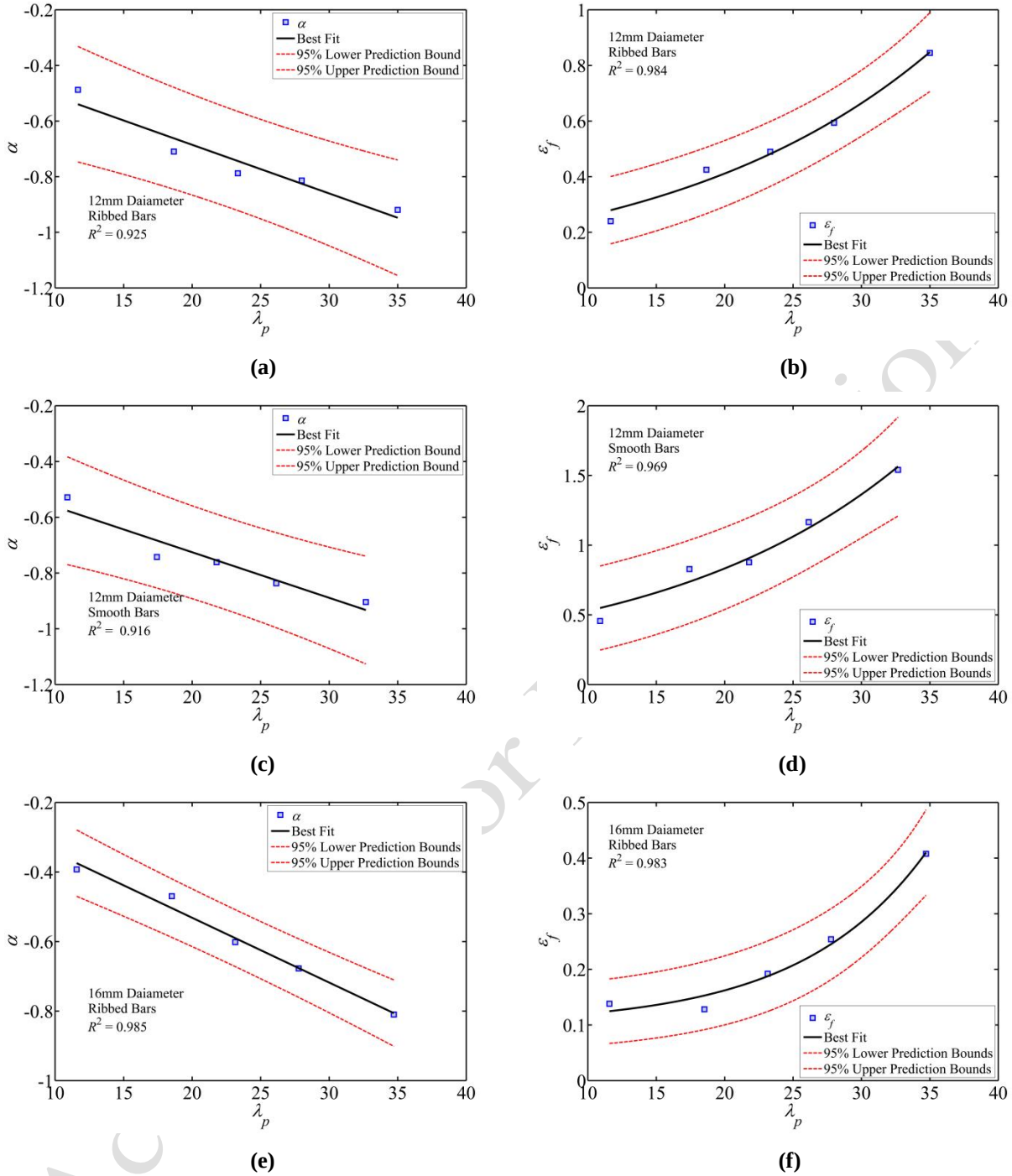

Fig. 14. Influence of non-dimensional slenderness ratio on fatigue material constants: (a), (c), (e) Impact of buckling on α and (b), (d), (f) Impact of buckling on ε_f

The relationship between the fatigue model parameters and λ_p is defined by empirical Eq. (4) and (5) which are the results of the regression analysis shown in Fig 14.

$$\alpha = a\,\lambda_p - b \tag{4}$$

$$\varepsilon_f = c\exp\left(d\,\lambda_p\right) + e \tag{5}$$

where, α and ε_f are the fatigue material constants, a, b, c, d and e are the regression coefficients that are shown in Table 4.

Table 4 The proposed fatigue material constants as a function of the λ_p

Material constants	*a*	*b*	*c*	*d*	*e*
12mm Dia ribbed bars					
α	-0.015	0.304			
ε_f			0.100	0.045	0.030
16mm Dia ribbed bars					
α	0.018	0.159			
ε_f			0.007	0.109	0.100
12mm Dia smooth bars					
α	-0.013	0.378			
ε_f			0.040	0.079	0.300

The results of regression analysis show that regardless of the reinforcement type (smooth or ribbed bars) by increasing the λ_p the ductility coefficient ε_f increases exponentially but ductility exponent α decreases linearly. The reduction in ductility exponent (α) is due to the increase in strain amplitude locally at the location of the plastic hinge in the bar due to buckling. This will result in premature crack initiation in bars with bigger λ_p. However, increasing the ductility coefficient (ε_f) means that the fracture strain of bar under once cycle increases by increasing the λ_p. The hysteretic response of bars previously shown in Fig. 3 indicates that the bars with bigger slenderness ratio after buckling in compression are not able to recover the stress in tension after load reversal with the same strain amplitude in tension. This is due the influence of geometrical nonlinearity and significant residual plastic deformation in compression. This indicates that mean strain has a big influence on the low-cycle fatigue life of reinforcing bars. The combined influence of inelastic buckling and mean strain is out of the scope of this paper and is an area for future.

Another important finding in this research is the influence of bar diameter on fatigue material constants. Fig. 15 shows a comparison between the fatigue material constants of 12mm and

16mm diameter ribbed bars as a function of λ_p. As expected the 16mm diameter bars have smaller low-cycle fatigue life compare to 12mm diameter bars. These results are in a good agreement with results observed by other researchers [3,16]. However, the influence of bar diameter increases by increasing the λ_p. This indicates that there is need for further study to explore the impact of bar diameter on low-cycle fatigue life of reinforcing bars with the effect of inelastic buckling.

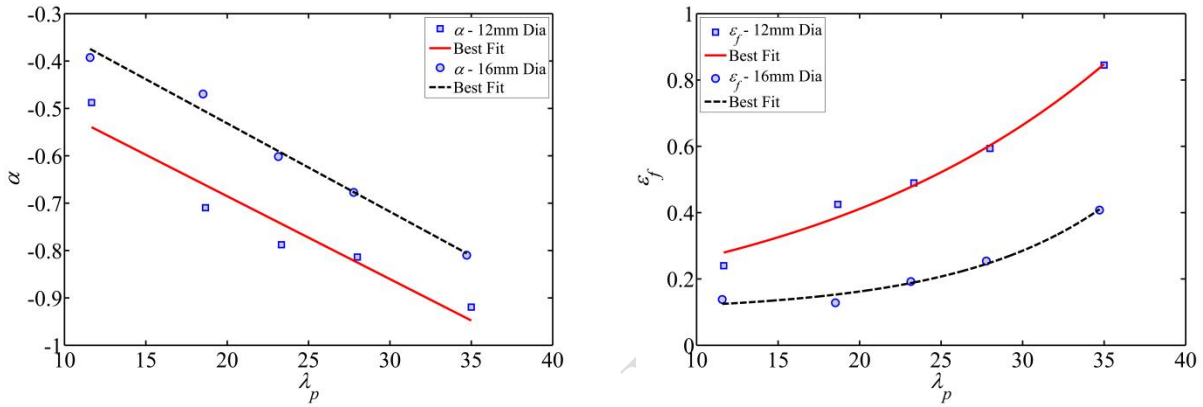

Fig. 15. Influence of bar diameter on fatigue material constants: (a) α, (b) ε_f

5. Analytical modelling

In recent decades the nonlinear analysis of RC framed structures subject to seismic loading has received a lot of attention. This has been focused on the development of the fibre element technique [14,25,26]. In this approach the member cross section is decomposed into a number of steel and concrete fibres at selected integration points. The material nonlinearity is represented through a uniaxial constitutive material model of steel (tension and compression) and concrete (confined core concrete and unconfined cover concrete). Kashani et al. [27] have developed a new phenomenological hysteretic model for reinforcing bars that includes the effect of inelastic buckling and low-cycle fatigue degradation. It should be noted that buckling is a second order effect due to the geometrical nonlinearity and large deformation. Unlike the old traditional uniaxial material models for reinforcing bars [28] this advanced material model combines the material nonlinearity due to yielding of steel with geometrical

nonlinearity due to buckling and low-cycle fatigue degradation into a single material model. This model has been validated against an extensive set of experimental and numerical simulation data of isolated reinforcing bars [6,7,24]. However, the fatigue material constants that were used in the model development were not calibrated to include the effect of buckling on fatigue material constants. Therefore, the experimental data generated in this paper improves this feature of the model to include the calibrated fatigue material constants as a function of λ_p. The detailed discussion of the model development and validation is available in [13,24]. In this section the model is only used to compare the improved analytical model with the observed experimental data.

A comparison between the improved model using the calibrated fatigue material constants (provided in Table 2) and the experimental results has been made and shown in Fig 16.

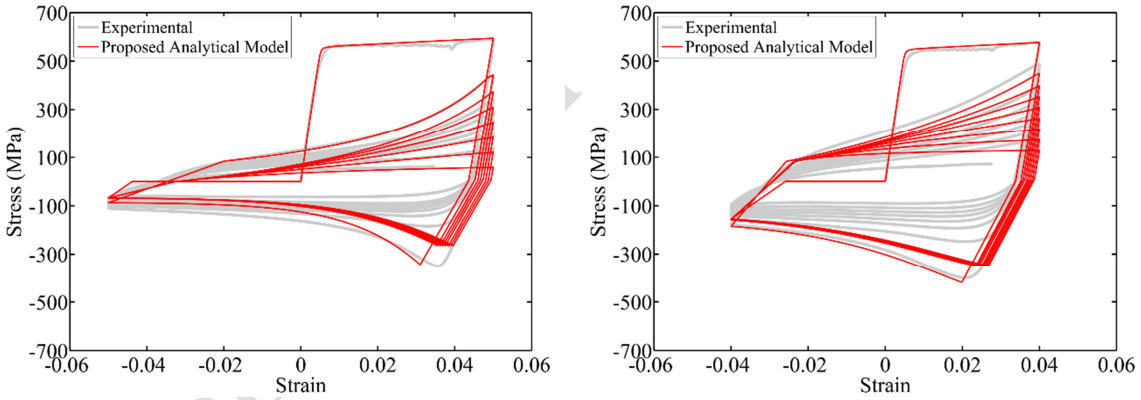

Fig. 16. Comparison of the proposed analytical model and the experimental results: (a) 12mm diameter bar with *L*/*D* = 15 at 5% strain amplitude (b) 16mm diameter bar with *L*/*D* = 10 at 4% strain amplitude

With reference to Fig 16, it is evident that the analytical model is capable of predicting the complex nonlinear behaviour of the reinforcing bars. It is also evident that the prediction of low-cycle fatigue degradation of reinforcing bars using the analytical model is in a good agreement with experimental results.

This is a very important contribution and improvement to the new material model developed by Kashani et al. [27]. The traditional material models are not able to simulate the combined

399 effect of inelastic buckling, material nonlinearity and low-cycle fatigue degradation.
400 Therefore, using the old material models in the seismic assessment and vulnerability analysis
401 of existing RC structures the seismic damage might be underestimated. Moreover, this
402 material model has already been implemented into the OpenSees. Therefore, it is readily
403 available for earthquake engineering community to be used in nonlinear seismic assessment
404 of RC bridges/structures.

405 **6. Conclusions**

406 A total of ninety constant amplitude low-cycle fatigue tests are conducted. The test
407 specimens were varied in lengths, diameter and surface condition (ribbed and smooth). Using
408 SEM technology the fractography of fractured surface is studied. The experimental data are
409 used to develop a new set of low-cycle fatigue model as a function of slenderness ratio and
410 yield strength of reinforcing bars. Finally, these empirical models implemented in to a new
411 phenomenological hysteretic model to simulate the nonlinear cyclic behaviour of reinforcing
412 bars.

413 The main outcomes of this study can be summarised as follows:

414 1) The inelastic buckling has a significant impact of the cyclic stress-strain behaviour of
415 reinforcing bars. As the buckling length of bars increased the low-cycle fatigue life
416 decreased and therefore, the energy dissipation capacity of the bars under cyclic loading
417 reduced.

418 2) The second order effect due to buckling increases the total strain amplitude at the internal
419 face of the buckled bars. Therefore, the low-cycle fatigue cracks initiates at the internal
420 face of the buckled bars and propagated through the bar.

3) The low-cycle fatigue tests showed that 16mm diameter bars have fractured earlier than 12mm diameter bars. Therefore, the bar diameter might influence the low-cycle fatigue life of reinforcing bars. This is a very important finding and is an area for future research.

4) As expected, the ribbed bars show a less ductile failure mechanism compare to smooth bars. However, as the buckling length of bars increases the influence of ribs reduces and fracture of bars is mainly governed by the stress concentration at the internal face of buckled bars which is due to the second order effect.

5) The results of SEM analysis showed that the fractured surface of smooth bars are much darker than ribbed bars. This indicates that the crack propagation process takes much longer than ribbed bars and therefore the fracture is more ductile.

6) The new low-cycle fatigue models have been implemented into a new phenomenological hysteretic model that simulates the cyclic stress-strain behaviour reinforcing bars. The model combines the geometrical nonlinearity due to inelastic buckling, material nonlinearity due to steel yielding together and low-cycle fatigue degradation in a single uniaxial material model. This advanced material model has been implemented into the OpenSees and is readily available to the earthquake engineering community to be used in nonlinear seismic analysis of RC bridges/structures.

Acknowledgements

The experimental work is funded by the Earthquake Engineering Research Centre (EERC) at the University of Bristol. The first author would like to thank Dr Nicholas Alexander of the University of Bristol for providing valuable guidance during the course of this research. Any findings, opinions and recommendations provided in this paper are only based on the author's view.

References

[1] El-Bahy A, Kunnath S.K, Stone WC, Taylor AW. Cumulative Seismic Damage of Circular Bridge Columns: Benchmark and Low-Cycle Fatigue Tests. ACI Struct J 1999; 96 (4): 633-643.

[2] Lehman DE, Moehle JP. Seismic performance of well-confined concrete columns. PEER Research Report 2000; University of California at Berkeley.

[3] Brown J, Kunnath Sk. Low cycle fatigue behavior of longitudinal reinforcement in reinforced concrete bridge columns. Technical Report MCEER-00-0007; 2000.

[4] Bae S, Mieses A and Bayrak O. Inelastic buckling of reinforcing bars. J Struct Eng 2005; 131 (2): 314–321.

[5] Kunnath SK, Heo Y and Mohle JF. Nonlinear uniaxial material model for reinforcing steel bars. J Struct Eng 2009; 135 (4): 335-343.

[6] Kashani MM, Crewe AJ, Alexander NA. Nonlinear stress-strain behaviour of corrosion-damaged reinforcing bars including inelastic buckling. Eng Struct 2013; 48: 417–429.

[7] Kashani MM, Crewe AJ, Alexander NA. Nonlinear cyclic response of corrosion-damaged reinforcing bars with the effect of buckling. Constr Build Mater 2013; 41: 388-400.

[8] Monti G, and Nuti C. Nonlinear cyclic behavior of reinforcing bars including buckling. J Struct Eng 1992; 118 (12): 3268–3284.

[9] Rodriguez ME, Botero JC and Villa J. Cyclic stress-strain behavior of reinforcing steel including the effect of buckling. J Struct Eng 1999; 125 (6): 605–612.

[10] Gomes A and Appleton J. Nonlinear cyclic stress-strain relationship of reinforcing bars including buckling. Eng Struct 1997; 19: 822–826.

[11] Dhakal R and Maekawa K. Modeling for postyield buckling of reinforcement. J Struct Eng 2002; 128 (9): 1139–1147.

[12] Dhakal R and Maekawa K. Path-dependent cyclic stress-strain relationship of reinforcing bar including buckling. Eng Struct 2002; 24: 1139–1147.

[13] Kashani MM. Seismic Performance of Corroded RC Bridge Piers: Development of a Multi-Mechanical Nonlinear Fibre Beam-Column Model, PhD Thesis 2014; University of Bristol.

[14] OpenSees, the Open System for Earthquake Engineering Simulation. (2011), PEER 2011; University of California, Berkeley.

[15] BS 4449-2005 +A2. Steel for the reinforcement of concrete - Weldable reinforcing steel - bar, coil and decoiled product – Specification; 2009.

[16] Mander JB, Panthaki FD, Kasalanati A. Low-cycle fatigue behavior of reinforcing steel. J Mater Civil Eng 1994; 6 (4): 453-468.

[17] Brown J, Kunnath Sk. Low-cycle fatigue failure of reinforcing steel bars. ACI Mater J 2004; 101 (6): 457-466.

[18] Higai T, Nakamura H and Saito S. Fatigue failure criterion for deformed bars subjected to large deformation reversals. ACI SP 237-4 2006; 237: 37-54.

[19] Hawileh RA, Abdalla JA, Oudah F and Abdelrahman K. Low-cycle fatigue life behaviour of BS 460B and BS B500B steel reinforcing bars. Fatigue Fract Eng M 2010; 33: 397-407. (39).

[20] Manson SS. Fatigue: A complex subject-Some simple approximations. Exp. Mech. 1965; 5 (7): 193–226.

[21] Koh SK, Stephens RI. Mean Stress Effects on Low Cycle Fatigue for a High Strength Steel. Fat Fract Eng Materi Struct 1991; 14 (4): 413-428.

[22] Chang GA, Mander JB. Seismic energy based fatigue damage analysis of bridge columns: Part I – Evaluation of seismic capacity. Technical report NCEER-94-0006, 1994.

[23] Miner MA. Cumulative damage in fatigue. J Appl Mech 1945; 12: A159–A164.

[24] Kashani MM, Lowes LN, Crewe AJ, Alexander NA. Finite element investigation of the influence of corrosion pattern on inelastic buckling and cyclic response of corroded reinforcing bars. Eng Struct 2014; 75: 113-125.

[25] Spacone E, Filippou FC and Taucer FF. Fibre beam-column model for non-linear analysis of r/c frames: part I: formulation. Earthq Eng Struct D 1996; 25: 711-725.

[26] Spacone E, Filippou FC and Taucer ff. Fibre beam-column model for non-linear analysis of R/C frames: part II: applications. Earthq Eng Struct D 1996; 25: 727-742.

[27] Kashani MM, Lowes LN, Crewe AJ, Alexander NA. Phenomenological hysteretic model for corroded reinforcing bars including inelastic buckling and low-cycle fatigue degradation. Comp & Struct 2015; 156: 58-71.

[28] Menegotto M, and Pinto PE. Method of analysis of cyclically loaded RC plane frames including changes in geometry and nonelastic behavior of elements under normal force and bending. Preliminary Report IABSE, Zurich 1973; 13: 15–22.

Appendix A. Low-cycle fatigue test results

Table A1. Low-cycle fatigue test results of 12mm diameter ribbed bars

L/*D*	Total Time (s)	Frequency (Hz)	Number of Half Cycles to Failure ($2N_f$)	Total Normalised Dissipated Energy (E_t/E_y)
1% Strain Amplitude				
5	3733.14	0.125	933	2835
8	1333.62	0.125	333	1489
10	887.13	0.125	222	1021
12	591.36	0.125	148	523
15	576.23	0.125	144	382
1.5% Strain Amplitude				
5	1991.08	0.083	332	2566
8	765.87	0.083	128	1120
10	596.83	0.083	99	613
12	488.72	0.083	81	398
15	428.51	0.083	71	294
2% Strain Amplitude				
5	1124.69	0.063	141	1831
8	506.56	0.063	63	649
10	409.95	0.063	51	429
12	361.01	0.063	45	312
15	426.05	0.063	53	267
3% Strain Amplitude				
5	607.52	0.042	51	1245
8	348.84	0.042	29	464
10	298.79	0.042	25	310
12	441.57	0.042	37	349
15	393.49	0.042	33	244
4% Strain Amplitude				
5	527.26	0.031	33	1094
8	366.02	0.031	23	458
10	267.21	0.031	17	289
12	425.70	0.031	27	314
15	363.16	0.031	23	231
5% Strain Amplitude				
5	402.91	0.025	20	846
8	328.22	0.025	16	414
10	328.61	0.025	16	303
12	323.06	0.025	16	246
15	330.17	0.025	17	220

Table A2. Low-cycle fatigue test results of 16mm diameter ribbed bars

L/*D*	Total Time (s)	Frequency (Hz)	Number of Half Cycles to Failure ($2N_f$)	Total Normalised Dissipated Energy (E_t/E_y)
1% Strain Amplitude				
5	4870.26	0.125	1218	3328
8	1364.69	0.125	341	1457
10	734.32	0.125	184	867
12	543.52	0.125	136	579
15	494.98	0.125	124	370
1.5% Strain Amplitude				
5	1937.77	0.083	323	2389
8	677.83	0.083	113	993
10	393.67	0.083	66	500
12	379.64	0.083	63	355
15	365.60	0.083	61	267
2% Strain Amplitude				
5	1050.74	0.063	131	1677
8	358.74	0.063	45	548
10	343.91	0.063	43	397
12	391.40	0.063	49	366
15	295.94	0.063	37	226
2.5% Strain Amplitude				
5	628.92	0.050	63	1205
8	289.43	0.050	29	438
10	267.66	0.050	27	318
12	265.82	0.050	27	258
15	312.27	0.050	31	231
3% Strain Amplitude				
5	558.47	0.042	47	1147
8	248.10	0.042	21	378
10	268.79	0.042	22	318
12	249.61	0.042	21	240
15	298.71	0.042	25	216
4% Strain Amplitude				
5	420.98	0.031	26	959
8	203.31	0.031	13	340
10	230.94	0.031	14	268
12	267.05	0.031	17	244
15	290.12	0.031	18	213

532 **Table A3. Low-cycle fatigue test results of 12mm diameter smooth bars**

L/*D*	Total Time (s)	Frequency (Hz)	Number of Half Cycles to Failure ($2N_f$)	Total Normalised Dissipated Energy (E_t/E_y)
1% Strain Amplitude				
5	10168	0.125	2452	5603
8	0.00	0.125	0	0
10	1944.38	0.125	486	1861
12	1530.27	0.125	383	1066
15	1117.62	0.125	279	604
1.5% Strain Amplitude				
5	4404	0.083	734	5603
8	1375.75	0.083	229	1500
10	1194.59	0.083	199	894
12	1120.97	0.083	187	679
15	1013.16	0.083	169	486
2% Strain Amplitude				
5	2937.79	0.063	367	4289
8	1096.16	0.063	137	997
10	1012.93	0.063	127	691
12	916.97	0.063	115	518
15	828.23	0.063	104	380
3% Strain Amplitude				
5	1659.46	0.042	138	2378
8	894.38	0.042	75	707
10	871.71	0.042	73	548
12	755.93	0.042	63	402
15	772.20	0.042	64	334
4% Strain Amplitude				
5	1287.05	0.031	80	1664
8	742.60	0.031	46	591
10	710.24	0.031	44	456
12	709.25	0.031	44	378
15	772.80	0.031	48	319
5% Strain Amplitude				
5	1018.59	0.025	51	1284
8	687.06	0.025	34	544
10	685.54	0.025	34	428
12	685.24	0.025	34	355
15	693.35	0.025	35	296

533
534